Compton Backscattering as a Means of Measuring the Beam Energy at the International Linear Collider

Desy Zeuthen Summer School
Project Report

Jörn Lange*

26 July - 19 September 2006

Abstract

Inverse Compton backscattering is a method currently being investigated in order to measure the beam energy at the ILC with high precision of $\Delta E_b/E_b = 10^{-4}$ or better. In this study, GEANT4 simulations are performed for a Nd:YAG laser of 1.165eV photon energy and a beam energy of 250GeV. A 3m long spectrometer magnet with B=0.28T is used to measure the Compton electron edge. However, the hereby created synchrotron (SR) radiation background causes problems for measuring the Compton photon peak's center of gravity with the required precision of about 1μm. Therefore, SR is included in the simulations and possible solutions, especially with respect to potential detector configuarations, are investigated. It is proposed to place an absorber close to a Si strip detector to convert the photons into e+/e-. For a thick absorber (20mm or above), this method seems to be promising to extract the Compton signal position accurately enough ($\leq 1\mu m$) despite the presence of background.

*Universität Hamburg, 20146 Hamburg, Email: joern_lange@gmx.de

1 Introduction

The accurate measurement of the beam energy is a basic requirement for precision experiments in high energy physics. This becomes especially important for threshold scans and particle resonance reconstruction. The future International Linear Collider (ILC) with beam energies around 250GeV is intended to measure particle masses, e.g. the ones of the top quark and the Higgs boson, with a precision in the range of 50MeV. This requires the incident e+/e- beam energy E_b to be known with a relative uncertainty of 10^{-4} .

A promising method, which is likely to become the standard of performing this task, is a beam position monitor (BPM) based spectrometer in a magnetic chicane [1]. However, it is desirable to have a complementary method available in order to have the possibility of cross-checking the measurement. Among the ones currently being investigated are the synchrotron radiation (SR) based method [2] and the Compton backscattering method. This study will focus on the latter one.

Measuring the beam energy by inverse Compton backscattering is not a novel technique and has already proved in practise, e.g. at BESSY, Berlin, [3] and at VEPP-4M, Novosibirsk [4]. But the beam energy there is only about a few GeV, which differs substantially from the one at the ILC. This requires to develop a complete different design and new detection methods. A good overview on the application of the Compton scattering method at the ILC can be found in [5] and [6].

The contribution of this study basically consists of performing first simulations of the Compton scattering technique with the aid of the software package GEANT4. Special attention has been given to the SR background by implementing SR into the GEANT4 simulations and analysing its inmpact on the Compton signal. With this knowledge, potential detector configurations have been investigated. In particular, the option of placing an absorber in the Compton photon beam in order to absorb SR and convert the Compton photons into easier measurable e+/e- pairs has been studied in detail.

2 Principle of Measuring the Beam Energy by Compton Backscattering

2.1 Inverse Compton Scattering

Compton scattering is defined as an elastic scattering process between an electron and a photon. The usual situation is the one of a photon scattering off from an electron at rest, which leads to an energy-momentum transfer from the photon to the electron so that the photon loses energy. But the situation here is the one of the so-called inverse Compton effect: A photon γ_L with energy ω_L scatters off from a high energy electron beam e_b:

$$e_b + \gamma_L \rightarrow e_{sct} + \gamma_{sct}$$

In this case, the photon gains substantial energy from the electron. The effect can be seen in Fig.1 which shows the energy distribution for the scattered electron (e_{sct}) and photon(γ_{sct}).

In order to exploit this process for beam energy measurements, it is important to note the sharp edge at minimum energy for electrons and at maximum energy for photons. The electron edge energy E_{edge} is related to the electron beam energy E_b as

$$E_{Edge} = \frac{1}{\frac{1}{E_b} + \frac{2\omega_L(1+\cos\alpha)}{m^2}}, \tag{1}$$

where α is the angle between the electron beam and the incident photons and m is the electron mass. Thus, if ω_L, α and m are known, measuring the edge energy yields the beam energy!

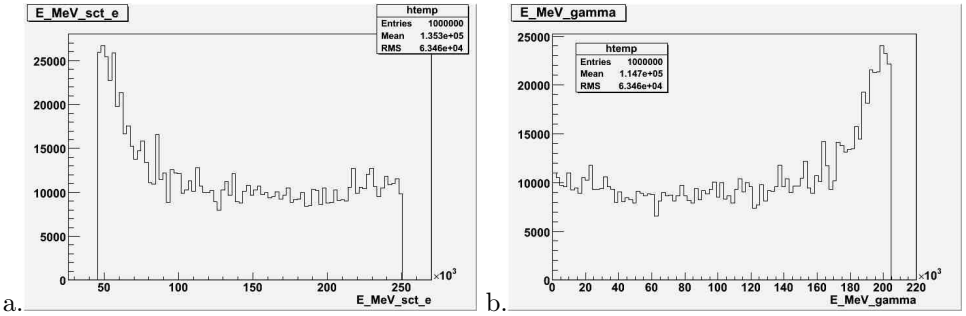

Figure 1: The energy distribution $\frac{dN}{dE}$ for (a) Compton scattered electrons and (b) photons. GEANT4 simulation for 10^6 events with $E_b = 250GeV$ and $\omega_L = 1.165eV$ (Nd:YAG laser).

2.2 Experimental Set-Up

How can the edge energy be measured? The low energy experiments using this technique measure the photon edge energy ω_{Edge} directly by means of high purity germanium (HPGe) detectors. However, the energies of the scattered photons at the ILC are completely different and their production rate is much higher so that HPGe cannot be used. The idea here is to measure the electron edge energy using a magnetic spectrometer. The sketch in Fig.2 shows this concept.

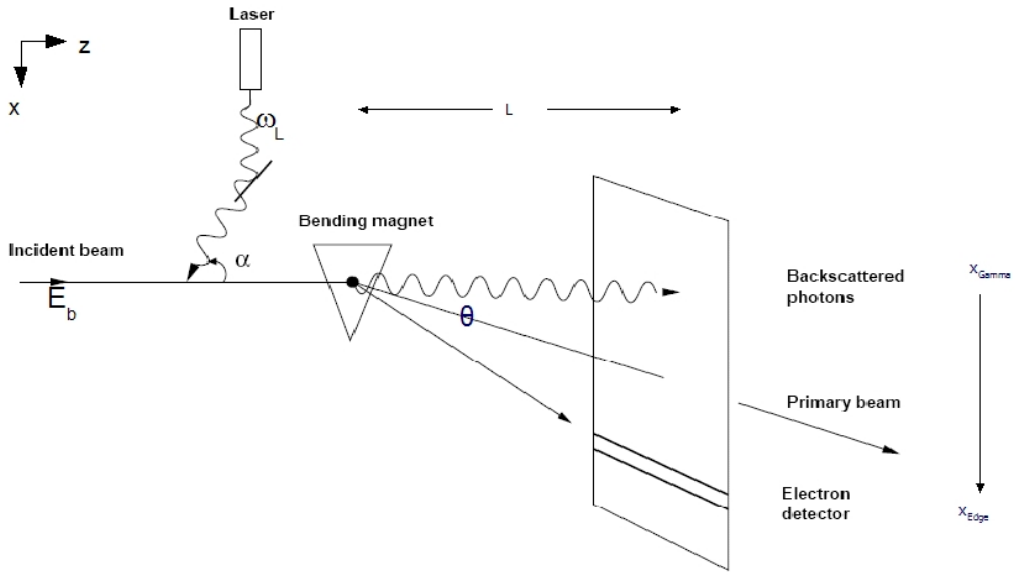

Figure 2: Sketch of the experimental set-up. Taken from [5] and modified.

A laser with energy ω_L is incident on the electron beam with energy E_b under the crossing angle α, which is close to zero for the real set-up. It is important that the technique is nondestructive, i.e. the majority of the beam electrons must not be affected! The event rate has to be chosen to fulfil this demand, which can be done by varying the laser intensity. On the other hand, there must be enough scattering to provide statistics. An ILC electron beam bunch is planned to consist of $2 \cdot 10^{10}$ electrons. A good compromise is to allow for $10^5 - 10^6$ electrons to interact. The scattered electrons and photons are highly collimated in the original electron beam direction and pass a bending magnet. The non-charged photons are unaffected and reach the detector after the distance L without change in direction so that their center of gravity x_{Gamma} should reproduce the original beam position at x=0. Both the unscattered beam electrons and the Compton scattered

ones, however, are separated by the bending magnet according to their energy. For low bending angles θ, the following equation relates the energy E to the offset x in the detector plane:

$$x = ec \cdot (L + \frac{l}{2}) \cdot \frac{B \cdot l}{E}, \tag{2}$$

where e is the electron charge, c the speed of light, B the magnetic field and l its length of the magnet in z-direction. Thus, the smaller the energy, the larger the offset. The unscattered beam electrons as the ones with the highest energy will be bent least, whereas the edge electrons undergo maximum bending. Knowing B and measuring the difference between the positions x_{Edge} and x_{Gamma} yields E_{Edge} via Eq.2, and so via Eq.1 finally E_b.

The beam energy precision mainly depends on the accuracy of B· l, L and $x_{Edge} - x_{Gamma}$. If $\Delta(B \cdot l)/(B \cdot l) = 10^{-5}$ and $\Delta L = 10\mu m$, which is expected to be achievable, it can be shown that $\Delta(x_{Edge} - x_{Gamma})$ has to be measured with micrometer precision in order to ensure a beam energy accuracy of$\Delta E_b/E_b = 10^{-4}$ [5].

3 GEANT4 Simulation Experiment

In this study, GEANT4 simulations were performed in order to investigate the behaviour of the scattered and unscattered particles and to find out if the precision requirements can be met. In particular, one special case was studied in detail: The electron beam moves with an exact, unsmeared energy of 250GeV at x=y=0 in z-direction. As the laser, Nd:YAG with $\omega_L = 1.165eV$ was chosen and brought to a nearly head-on collision with the electron beam ($\alpha = 8mrad$). Since GEANT4 does not provide an event generator for Compton backscattering, the expected energy distribution of the scattered photons was calculated beforehand and given to GEANT4 as an input file. From this the scattering angle θ_{sct} and the energy distribution of the scattered electrons could be calculated by kinematics, whereas the angle ϕ was created randomly according to a uniform distribution. So in fact, there were three different "final state" particles implemented in GEANT4: The unscattered beam electrons, the Compton scattered electrons and the Compton scattered photons. It will be important to distinguish between these three! Usually, for one simulation 10^6 events were generated, which corresponds to the number of scattered particles per bunch. To account for the much higher number of unscattered beam electrons per bunch, their results were scaled up afterwards by a factor of $2 \cdot 10^4$. The bending magnet was implemented with $l = 3m$ a magnetic field of $B = 0.28T$ in y-direction. After travelling $L = 50m$ through a vacuum chamber, the properties, i.e. x, y, z, E, of all particles have been evaluated at the assumed detector position.

4 The Electron Edge

For the configuration described, an offset of $x_b = 5.2cm$ for the beam electrons and $x_{Edge} = 28.3cm$ for the edge electrons is expected. Fig.3a shows that the simulation reproduces this value well.

The edge is very sharp because simulations were done without considering e.g. beam energy and position variations. But in reality these effects occur, so that the edge will be smeared over a certain range. This smearing is expected to be Gaussian. The edge position can then be obtained by fitting the data histogram in the edge vicinity with a convolution of a step function, which describes the edge, and a Gaussian, which allows for the smearing. For a more general case of one linear function to the left and one to the right of the edge, respectively, the function can be written:

$$f(t)_{a,b,c,d,x_0,\sigma} = \frac{\sigma}{\sqrt{2\pi}}(c-a)e^{-\frac{(t-x_0)^2}{2\sigma^2}} + \frac{1}{2}((a-c)(t-x_0)+(b-d))\text{erfc}(\frac{t-x_0}{\sqrt{2}\sigma}) + c(t-x_0) + d, \tag{3}$$

with the parameters a and b (gradient and constant of the linear function left), c and d (gradient and constant of the linear function right), x_0 (position of the edge) and σ (standard deviation of

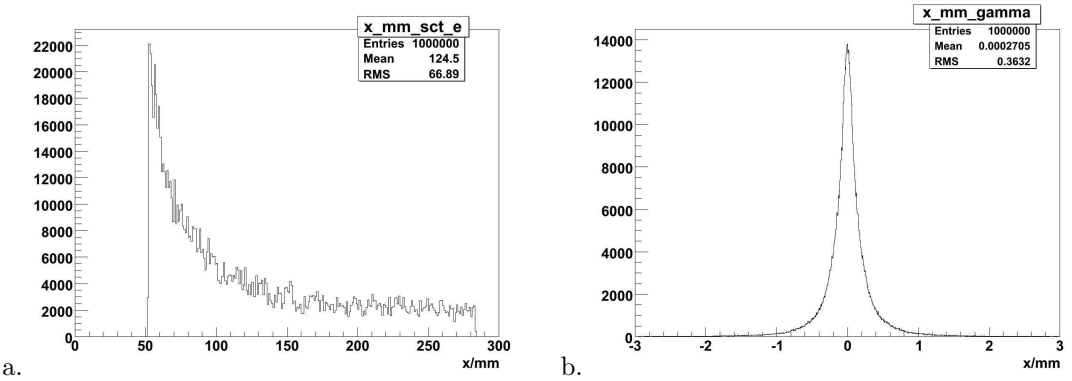

Figure 3: The $\frac{dN}{dx}$ distribution for (a) the scattered electrons (1mm bin) and (b) the Compton photon peak (5μm bin). 10^6 events generated.

the Gaussian). A detailed derivation of Eq.3 can be found in the appendix. GEANT3 simulations including smearing and using the $C0_2$ laser [6], have already shown that the above function fits the data well. Moreover, the edge position obtained from the fit was to a great extent independent from the bin width up to 100μm so that possibly detectors with up to 100μm segmentation can be used. Silicon (Si) strip detectors seem to be a reasonable choice.

However, one problem can be seen from the simulation results using the Nd:YAG laser presented here. The energy distribution $\frac{dN}{dE}$ of the scattered electrons as shown above in Fig.1a has a significant peak at E_{Edge} due to enough statistics at the edge. But the situation for $\frac{dN}{dx}$ at the edge electron position x_{Edge} is exactly opposite, i.e. only a relatively small amount of events, which is an effect due to the antiproportional relation between x and E ($x \propto \frac{1}{E}$). Fig.3a makes clear that there are only about 2000 entries for the 1mm bins around the edge. For sensible detector bins of e.g. 50μm width, this means that only in the order of 100 events are expected resulting in poor statistics with a lot of fluctuation around the edge. To conclude, for better statistics at the edge, it is necessary to either take the CO_2 laser or to produce more Compton backscattering events by enlarging the luminosity. The latter solution, however, will encounter soon its limit because the energy monitoring should be nondestructive to the electron beam.

For further studies, the beam energy and position variations resulting in smearing should be also included into GEANT4 simulations.

5 The Compton Photon Peak

Having analysed the results of the simulation concerning the electron edge, let us now turn to the Compton photon peak, whose center of gravity is expected to account for the original electron beam position. As we know that the beam position in these simulations is set exactly to x=0, the challenge now is to check if the Compton peak is also centred at 0 and to find a method how to obtain this position and its uncertainty. Fig.3b shows the simulation result of the Compton peak, which is indeed highly centred around 0. The mean of the data histogram is $x_{Gamma} = 0.27\mu m$. Due to not yet considered background, it will be however necessary for real measurements to fit the histogram appropriately. The next section will deal with the probably most dominant background, the SR, and develop adequate fitting techniques which allow to extract the position of the Compton signal with the precision required.

5.1 Synchrotron Radiation Background

When electrons pass through a magnet with the B-field perpendicular to their direction of motion, photons known as synchrotron radiation are emitted. Consequently, this effect has to be taken

into account as a potential background of the Compton photon signal. Basic features of the SR produced by the unscattered beam electrons in GEANT4 simulations are presented in Fig.4. The photon multiplicity per electron in Fig.4a reveals to be between 0 and 15, with average number $< N_{SR} >= 5.192$. This agrees perfectly with the theoretical expection of $< N_{SR} >= \frac{5}{2\sqrt{3}} \frac{\alpha e B \cdot l}{mc} = 5.192$, where α is the fine structure constant. This makes clear that there is, unlike in GEANT3, no cut-off for SR photons at low energies in GEANT4. This also becomes apparent from the energy distribtion in Fig.4b. The photons are produced with an energy ranging from values as low as $10^{-12} eV$ up to $100 MeV$ with an average energy of $< E_{SR} >= 3.579 MeV$. Again this is in perfect agreement with the estimated value $< E_{SR} >= \frac{8\sqrt{3}}{45} \cdot E_{critical}$, where the critical energy is defined as $E_{critical} = 0.65 \cdot E_b^2[GeV] \cdot B[T] = 11.64 MeV$, and the shape of the curve is also as expected (cf. [7]).

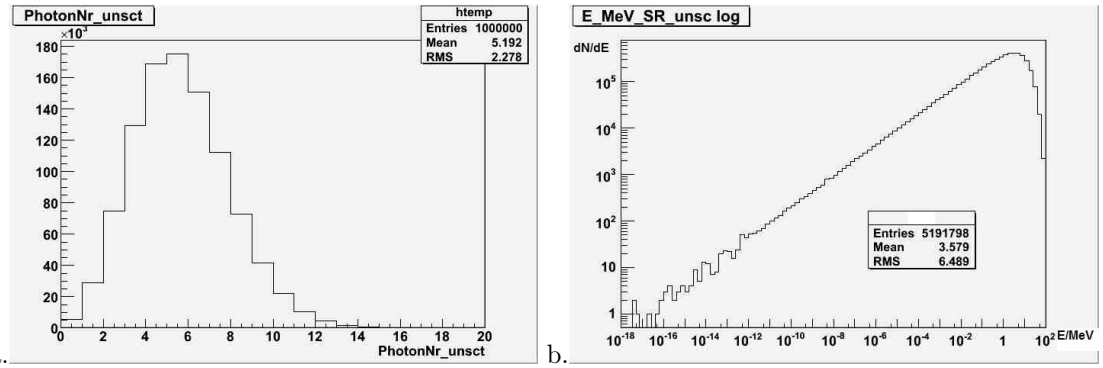

a. b.

Figure 4: Basic features of the SR produd by 10^6 unscattered beam electrons in the magnet as simulated in GEANT4: (a) The multiplicity of SR photons, (b) The energy distribution $\frac{dN}{dE}$ in a double-logarithmic scale.

The photon multiplicity for the SR produced by the Compton scattered electrons is exactly the same since $< N_{SR} >$ is only dependent on the magnet configuration. But the SR energy distribution is slightly changed due to the lower and widely distributed energy of the scattered electrons. The mean energy of the SR photons is shifted to the lower value of $< E_{SR} >= 1.284 MeV$. Also the x distribution of SR from the scattered electrons differs substantially from the one of the beam electron. Whereas the unscattered electron SR fan is more or less uniformly distributed between x=0 and x=5.2cm, the SR fan from the scattered electrons first behaves similarly, though on a lower level, upto x=5.2cm, but then it drops over a long distance to zero at x=28.3cm (see Fig.5).

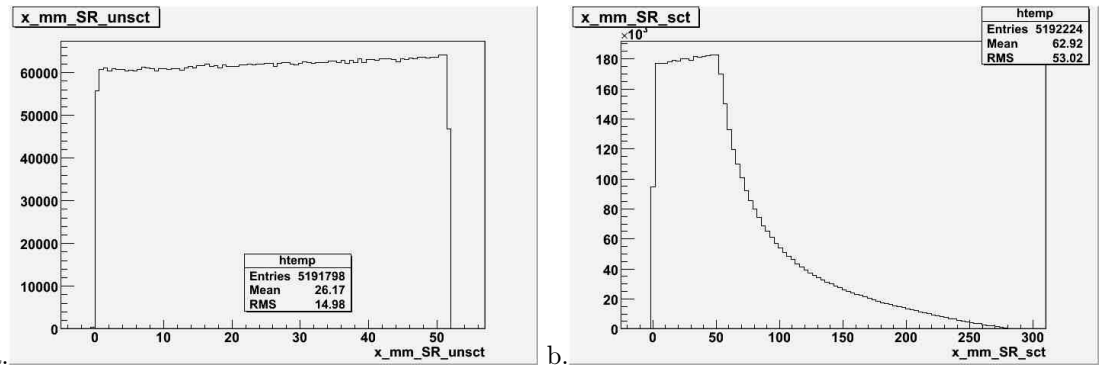

a. b.

Figure 5: The x distribution $\frac{dN}{dx}$ of the SR fan: (a) from the unscattered electrons, (b) from the scattered electrons. 10^6 events.

Now comes the decisive part concerning analysing the impact of SR on the photon signal. The simulations were done only for 10^6 events of unscattered electrons as well as for 10^6 scattered electrons and Compton scattered photons. For the Compton backscattered particles, this number of events per bunch is in the right order for a realistic ILC beam energy measurement. But since there will be about $2 \cdot 10^{10}$ particles per electron bunch, this also implies $2 \cdot 10^4$ more SR photons from the unscattered electrons, and consequently, the number of the beam electrons and their associated SR photons has to be scaled up by this factor. This will result in an enormous rate increase of SR background. In Fig.6, the x distributions for the individual signals (only beam electron SR, only scattered electron SR, only Compton scattered photons) are juxtaposed in the region around x=0. In Fig.6d, they are plotted together in one diagramme with logarithmic scale in order to compare their sizes. It turns out that due to the vast amount of beam electrons, their associated SR clearly dominates. This radiation yield is about 3 orders of magnitude larger than the one of the Compton photons near their center of gravity, which makes it impossible to determine x_{Gamma}.

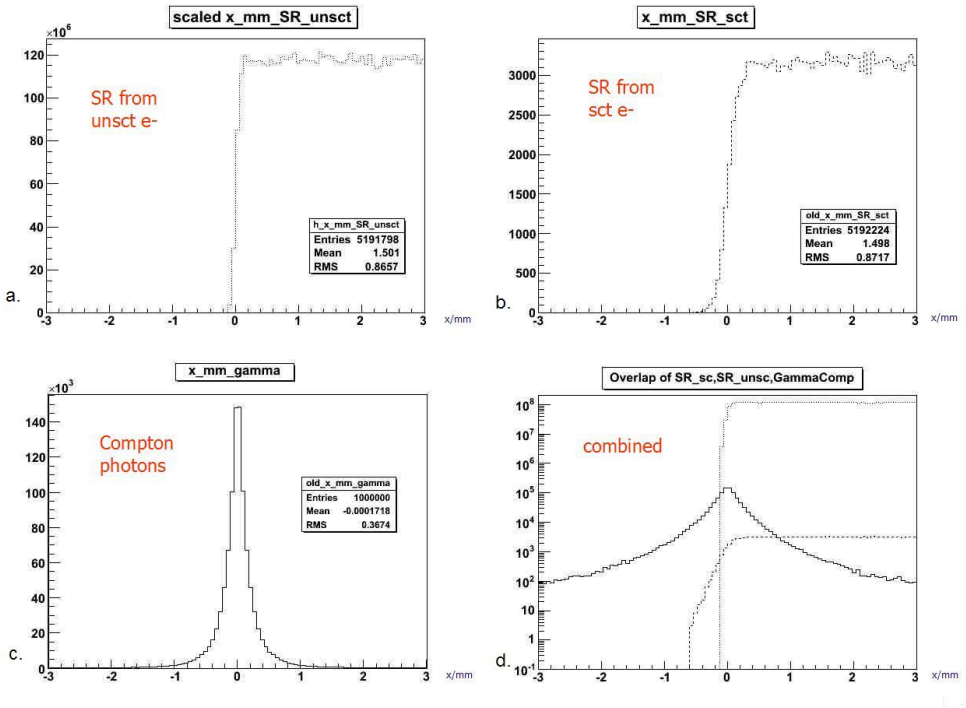

Figure 6: The x distributions $\frac{dN}{dx}$ around x=0 for (a) only beam electron SR, (b) only scattered electron SR and (c) only Compton scattered photons. All simulations performed for 10^6 events, but the distribution in a. has been scaled up to $2 \cdot 10^{10}$ events. In (d) all three previous curves are superposed, logarithmic y-axis.

But because of the very different energy ranges (GeV for Compton photons, MeV for SR), the situation looks much better for $\frac{dE}{dx}$ as seen in Fig.7). Now the Compton photon peak is clearly dominating with only a very low background signal for x>0 due to the beam electron SR. However, even this weak background has to be taken into account for precise x_{Gamma} measurements. This was tried to be done by developing different fitting techniques.

First of all, we have to find out which function fits the pure Compton peak signal best. As seen in Fig.8, the Gaussian and the Lorentzian functions do not fit the data well according to the χ^2/ndf, neither does the Voigt fit, which is a convolution of both. It was found that the a better fit to the Compton peak was produced by the product of Gaussian and Lorentzian. But for our goal of fitting, i.e. obtaining the mean position x_{Gamma} of the signal, all ansatzes tried were acceptable. Although the means of the Lorentzian and of the product of Gauss and Lorentz

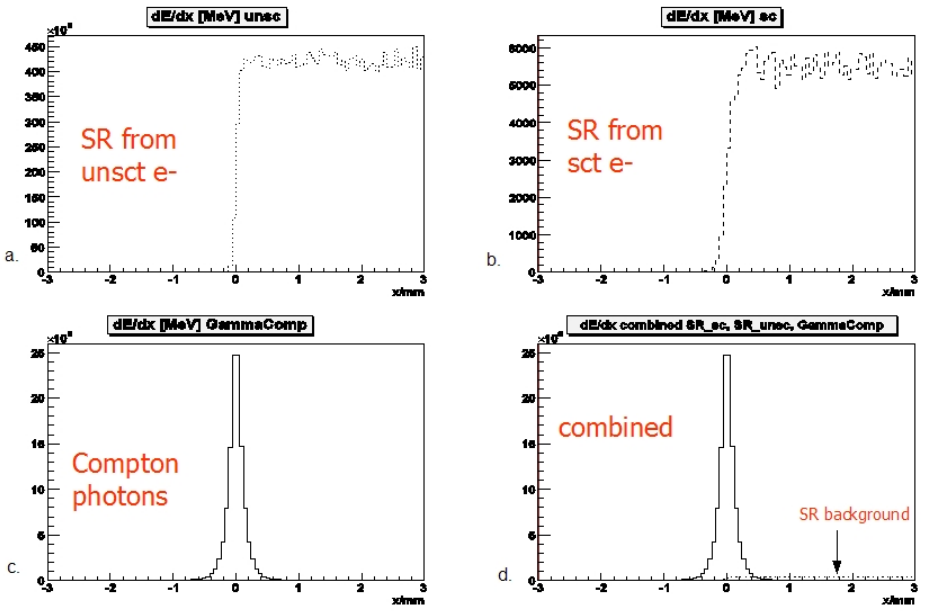

Figure 7: The $\frac{dE}{dx}$ distributions around x=0 for (a) only beam electron SR, (b) only scattered electron SR and (c) only Compton scattered photons. All simulations were performed for 10^6 events, but the distribution in (a) has been scaled up to $2 \cdot 10^{10}$ events. In (d) all three previous curves are superposed and presented with logarithmic scale.

were usually a bit closer to x=0, even the Gaussian could be used for this purpose. The result was always dependent on the interval of fitting and the bin width, but in general, the mean of the fits were always in the order of 0.05μm up to a few 0.1μm. This is well within our precision limit.

In the case of Compton peak plus SR backgroud, fitting over a wide range, e.g. x=[-3,3]mm, led to very bad results because the background is asymmetrically on the right side. But cutting off the tails and fitting only the core zone arond x=0, led to quite promising results. The means usually were in the range around 1μm. However, much better results could be obtained by implementing the background into the fit. The way it was done, was to add to the normal peak function a fixed constant for $x > x_{mean}$ accounting for the background. This constant had been obtained by an independent fit over x=[2,3]mm because we expected that in this region, the Compton peak is essentially zero so that only background exists there. The example in Fig.8d, where the product of Gaussian and Lorentzian had been chosen as the peak function, resulted to $x_{Gamma} = -0.03\mu m$, which is extremely close to x=0. So by this method, the center of gravity of the Compton photons could be obtained with sufficient precision despite the SR background.

5.2 Detector for the Compton Backscattered Photons

In the section above, we have discussed the properties of the photons and their distributions at the detector position, but without any detector specification. Let us now consider which detector would be suitable. As we have seen, due to SR background, it is impossible to determine the position of the Compton photon peak by measuring the photon rate $\frac{dN}{dx}(x)$. But a Photon calorimeter to measure the photon energy, $\frac{dE}{dx}(x)$, would be a good option. But such detectors currently available have a granularity in the range of $1mm$, which would be too large by a factor of 10-20 because the Compton photon signal is only extended over a region of approximately $2mm$. So further R&D would be needed in this field.

The approach discussed here is a different one. An absorber is placed in the Compton photon yield in front of the detector, which will have two effects: First, a large part of the SR background will be absorbed, and second, the high energetic Compton photons will convert to a great extent

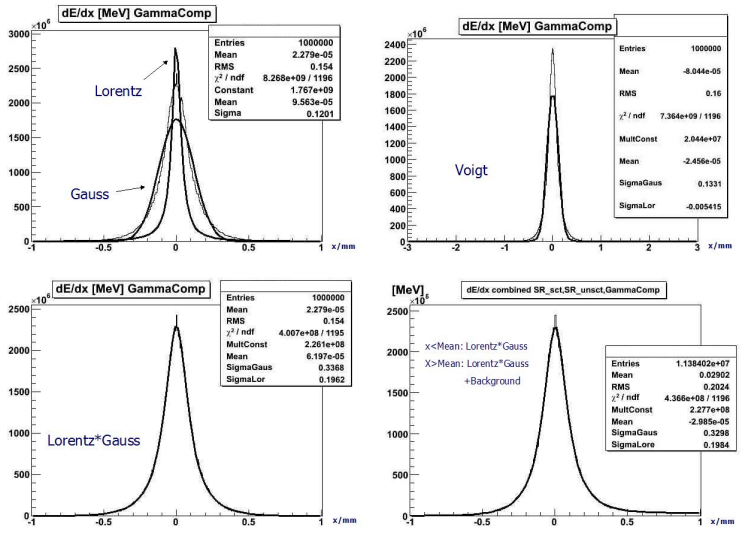

Figure 8: Different fits to the photon peak. The Compton photon peak is fitted with a Lorentzian and a Gaussian in (a), with a Voigt fit in (b) and with the product of Gaussian and Lorentzian in (c). The superposition of the Compton peak with the SR background is fitted with the product of Gauss and Lorentz + a background constant for $x > x_{mean}$ in (d).

into positron/electron (e+/e-) pairs, which can be measured by e.g. Si strip detectors with high precision. It will be shown that the center of gravity of the secondary[1] e+/e- is in high accordance with the position of the primary Compton photons.

5.3 Absorber

In order to choose a suitable absorber, it is important to understand the interactions of photons and electrons/positrons with matter. In the set-up proposed, there are two different categories of photons with different energy regimes incident on the absorber.

On the one hand, the Compton photons have energies in the range of many GeV and thus undergo basically only conversion into e+/e- pairs, which is the dominant process for photon energies larger than some MeV. The created e+/e- pairs also have mostly energies in the order of a few GeV. Thus, most of them survive ionisation, bremsstrahlung and multiple scattering processes inside the absorber and, moreover, produce additional e+/e- and photons in electromagnetic showers.

In contrast, the SR background has energies far below $1GeV$ with a peak at a few MeV. Its high energy tail is also able to produce e+/e- pairs, but most of the SR interact through Compton scattering ($E_{Photon} = 100keV - 10MeV$) or photoelectric effect ($E_{Photon} < 100keV$). The secondary electrons or positrons produced are usually too weak in energy to survive so that the vast majority of them is absorbed in the material. However, as we will see later, due to the giant amount of SR produced by the beam electrons, this tiny fraction (per photon) that leaves the absorber is not negligible and has to be taken into account.

An optimum absorber converts the Compton photons efficiently and without too much change in direction into e+/e- pairs and allows enough of those to reach the detector. On the contrary, for the lower energetic secondary electrons produced by the SR background, it is highly desirable to have them absorbed as much as possible to minimise the background. As the conversion rate for photons and the absorption rate for electrons become larger with increasing atomic number

[1] In the following, all particles created in the absorber (i.e. including also tertiary particles and so on) will be referred to as "secondary", regardless of their real production level.

Z, absorption materials with large Z are favourable. In our study, lead (Pb, Z=82) was chosen as the absorber medium.

In order to study the effect of an absorber on both the Compton photons and the SR photons in detail, Geant4 simulations were performed with varying absorber thickness. A Pb block with a cross section of 4cm x 2cm in the x-y plane and thicknesses of 4mm, 7mm, 10mm, 15mm and 20mm was taken. It was placed directly adjacent to the detector and perpendicular to the Compton backscattered photons. Again the simulations were done for 10^6 Compton backscattered events and unscattered beam electron.

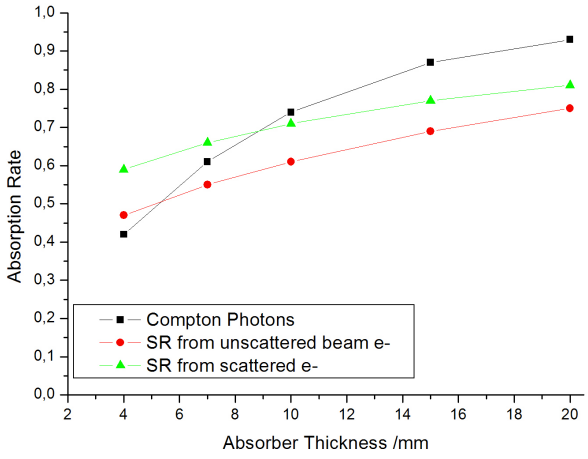

a.

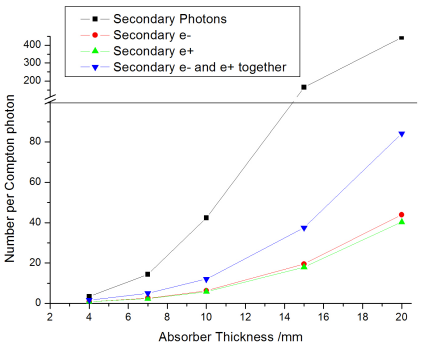

b.

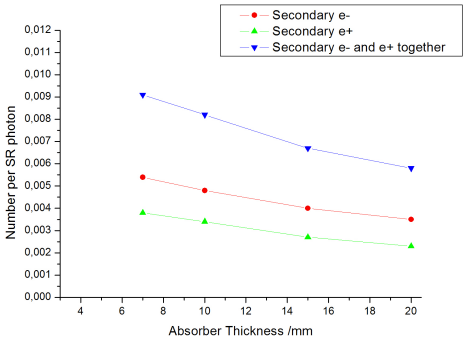

c.

Figure 9: Absorber properties as a function of its thickness:
(a) The absorption rate of Compton photons, SR from the unscattered beam electrons and SR from the scattered electrons.
(b) The number of secondary e+, e- and photons produced per incoming Compton photon and leaving the absorber.
(c) The number of secondary e+ and e- produced per incoming SR photon from the unscattered beam electrons and leaving the absorber.

Let us first study some properties of the absorber material. Fig.9a shows the absorption rate as a function of the material thickness, i.e. the number of photons which have been absorbed, normalised to the number of incoming photons. It can be clearly seen that, as expected, the absorption rate rises with increasing material thickness. It is interesting to note that for a thin absorber, less Compton photons than SR photons are absorbed, whereas for large absorber thickness, the opposite is true. In the focus of interest, however, is the outcome of secondaries from the absorber. In Fig.9b the number of e+/e- and secondary photons created by one incoming Compton

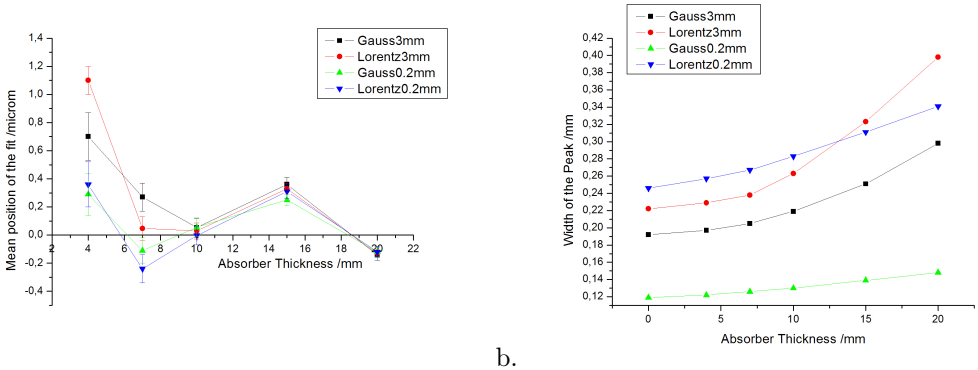

a. b.

Figure 10:
(a) The mean position of the different fits to the e+/e- peak (5μm bin) as a function of the absorber thickness.
(b) The width of the different fits as a function of the absorber thickness. Thickness "0" indicates the width of the primary Compton photon peak without absorber.

photon is shown and in Fig.9c compared to the number of secondaries created by one incoming SR photon. These two plots behave in a very different way: The number of e+/e- produced per Compton photon is about 3-4 orders of magnitude larger than the one produced per SR photon. Moreover, the number of secondaries from the Compton photons rises significantly with increasing thickness, whereas the number of secondaries from the SR decreases but less fast. Consequently, the best signal to background relation is expected for the 20mm thick absorber.

The growing e+/e- signal implies an increasing radiation problem for the detector. Assuming an energy deposit of only e+/e- with minimum ionisation inside the detector (which is valid for $E_{e+/e-} > 1MeV$), an energy loss of approximately $-\frac{dE}{dx} = 4.6\frac{MeV}{cm}$ in Si ($\rho = 2.3\frac{g}{cm}$) is expected. Therefore, a particle would deposit 0.14MeV inside a 300μm thick detector. Multiplied by the total number of produced e+/e-, this gives 1.67TeV per bunch for 10mm absorber thickness or 11.6TeV for 20mm. Considering the 2820 bunches per train with a frequency of 5 Hz, this gives a power of 3.8mW for the 10mm or 26.3mW for the 20mm absorber, which is incident on the detector over an area of not much more than $1mm^2$. However, this estimation does not account for the background, which will provide an additional deposit at least in the same range.

The most important question is whether the secondaries produced by the Compton photons in the absorber reproduce the center of gravity of their parent particles with μm precision. In the following, we will be focuse on e+/e- because the photons are expected not to create a significant signal in the Si strip detector[2]. Furthermore, if not specified otherwise, we will always refer to the x distribution of the number of particles, $\frac{dN}{dx}$, because minimum ionising particles result in an energy-independent signal. Thus, the total detector signal will be proportional to the number of passing particles.

The e+/e- peak has been fitted with a Gaussian and a Lorentzian for two different intervals: [-3,3]mm and [-0.2,0.2]mm. The results for the mean positions of the different fits are illustrated in Fig.10 as a function of the absorber thickness. The fit for 4mm absorber seems to be significantly worse than the ones for larger thicknesses. Although the fitted position varies slightly with the absorber thickness, there is no clear dependence noticeable, independent from the fit procedure. In general, the position evaluated from the e+/e- particles agrees very well with the one of the primary Compton photons. The deviation from 0, which is the true position of the original electron beam, is generally a few tenth of a μm and therefore well below the intended precision limit. The width of the peak, however, depends on the absorber thickness (cf. Fig.10b) and becomes larger with increasing thickness, as expected. For all the results discussed, a bin width of 5μm has been

[2]The mean free path of photons with an energy $> 100keV$ is about 5cm in Si so that a 300μm thick Si strip detector absorbs only 0.6% of them.

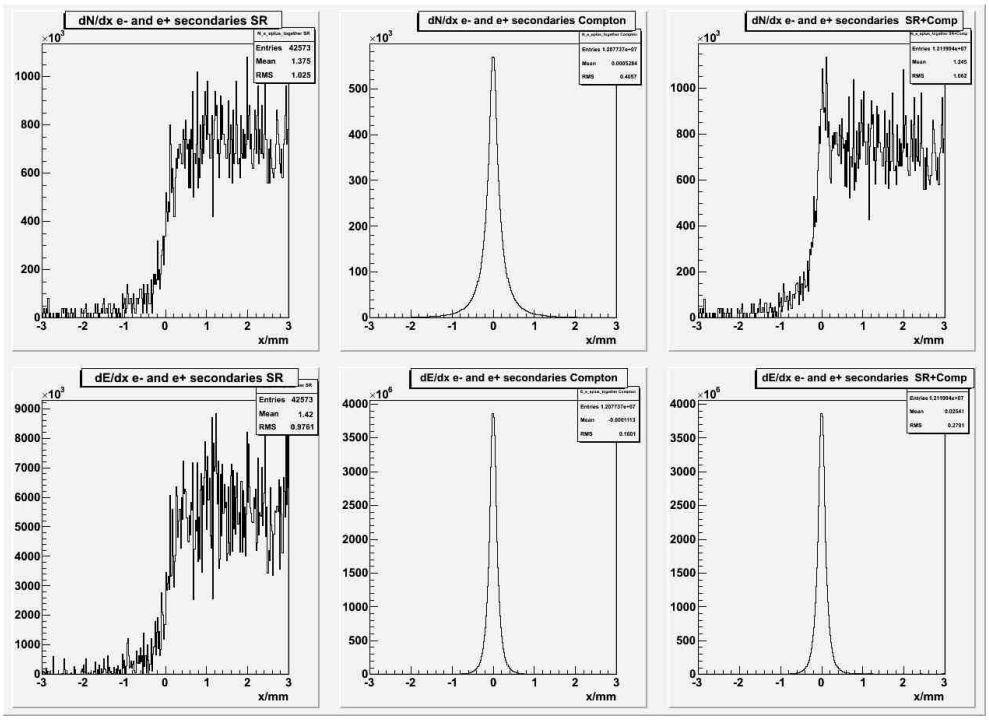

Figure 11: The spectra $\frac{dN}{dx}$ (top) and $\frac{dE}{dx}$ (bottom) of the secondary e+/e- produced in 10mm Pb absorber; left: e+/e- produced only by the SR (scaled up); middle: e+/e- only from Compton photons; right: the combined signal. 20 μm bins.

chosen, which corresponds to the pitch of a novel Si strip detectors. However, it might be cheaper and safer to rely on established detectors with a larger pitch of e.g. $25\mu m$. Investigations revealed that the fitted peak position was independent on bin widths of 5, 20, 50 and 100 μm.

So far only e+/e- particles from Compton photons have been studied and shown that their center of gravity has no significant offset compared to the original Compton peak. However, also the SR photons interact in the absorber and produce e+/e- particles. Although most of them do not leave the absorber, as shown above, the surviving fraction has some impact after scaling up by $2 \cdot 10^4$. Fig.11 shows the situation for a 10mm absorber, where the outcome of e+/e- from the SR is in the same order as the one from the Compton photons (per bin, in the peak region). For thinner absorbers, the background dominates the signal. However, the situation for thicker absorbers is considerably better, see e.g. Fig.12 for the 20mm absorber. Here, the signal exceeds the background clearly. But again, the question is whether the center of gravity of the peak can be determined with sufficient precision despite the background.

The idea here is the same as for the primary SR background problem discussed in chapter 5.1: the combined signal was fitted with the sum of the peak and background. As the peak fit function the Lorentzian has been chosen, and for the e+/e- from the SR, it was found that the edge function from Eq.3 provided also a very good description. Some attempts have been made to fit the combined signal without fixing the edge function's parameters. The results were in the range of $x_{mean} = 1 - 10\mu m$ and the fit varied significantly with the fit interval chosen and on its start parameters. But when the background is measured independently, it can be fitted with the edge function and the resulting paramters were kept as fixed in the subsequet overall fit. Only the parameters of the peak function remained variable during the final fit. This fitting procedure turned out to be more stable and precise: x_{mean} was usually in the range of 0.5...1μm. If this technique is used for the real experiment, the e+/e- background signal has to be known precisely and measured independently. This can be achieved if the laser is turned off and no Compton backscattering occurs. Further investigations are however needed to see if the e+/e- signal from

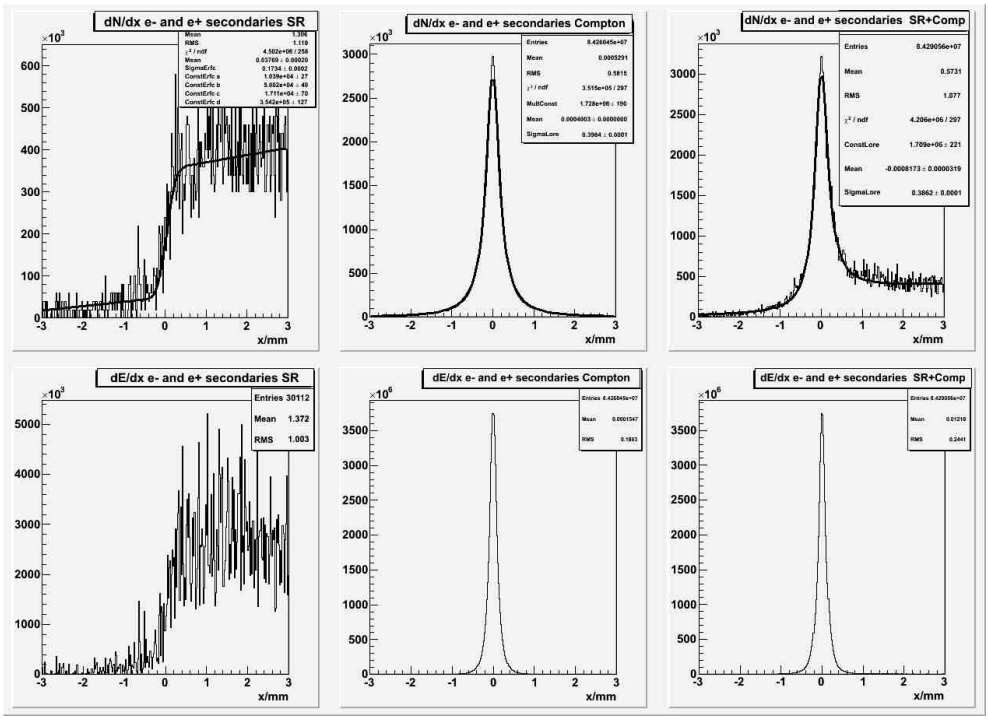

Figure 12: The spectra $\frac{dN}{dx}$ (top) and $\frac{dE}{dx}$ (bottom) of the secondary e+/e- produced in 20mm Pb absorber; left: e+/e- produced only by the SR (scaled up, fitted with the edge funtion from Eq.3); middle: e+/e- only from Compton photons (fitted with a Lorentzian over [-3,3]mm); right: the combined signal (fitted with the sum of the two previous functions with fixed parameters for the edge function). 20 μm bins.

the SR does not differ too much from bunch to bunch.

The best way, however, to cope with the e+/e- background problem would be to eliminate the background, at least to a reasonable extent. The analysis so far has revealed that one solution is increasing the absorber thickness. More simulations with larger thicknesses would be desirable. Figs.11 and 12 (bottom) indicate another possibility which relies on the $\frac{dE}{dx}$ distribution of the e+/e- particles. Again, it would be advantageous to have a calorimeter instead of a rate counter. However, an electron calorimeter with desired properties is not yet known. But what about an energy filter? The e+/e- produced by the SR usually have an energy up to 10MeV, with a low intensity tail up to 50MeV. Their mean energy value is $< E_{mean} >= 6.7MeV$ after passing a 20mm absorber. In contrast, the e+/e- produced by the Compton photons have energies up to a few GeV with $< E_{mean} >= 782.4MeV$. A bending magnet should be able to sweep a considerable amount of he e+/e- background away, while the high energy signal particles should be hardly affected. In particular, the magnet must not change their x distribution requiring the B-field to be aligned along the x-axis in order to bend the particles into y-direction. A 10cm long magnet with 0.5T, as an example, affects most of the background e+/e-. It results to an offset of $\Delta y = 1.5cm$ for 50MeV particles, and even more for e+/e- with lower energies, whereas the higher energetic e+/e- produced by the Compton photons would be influenced only very slightly. The magnet dimensions are somewhat restricted since in the discussed set-up, the unscattered electron beam has an x-offset of only 5.2cm and should not be influenced by an additional B-field.

In the end of this section, some considerations on the limitations of the models and simulations used should be mentioned:

- GEANT4 uses a so-called range-cut with regards to the production of secondaries in particle interactions. This means that only secondary particles are produced which are expected to

travel a greater distance inside the respective material than the set cut value. The default cut value, that was used here, is 1mm. This implies for our absorber material Pb that photons with energies less than 100.5keV, e- with energies less than 1.38MeV and e+ with energies less than 1.28MeV are not produced in the absorber. So although their energies are small compared to the actually produced particles, they should be better accounted for because these low energy particles have complicated interaction cross-sections with matter.

- So far, only the e+/e- production in the absorber has been considered. Secondary photons produced by the Compton photons in the absorber play only a minor role in the detector. Moreover, like the e+/e-, their center of gravity is expected to reproduce the Compton peak, too. But what about the influence of the secondary photons created by the SR? Further research should be done to check if their influence has to be taken into account.
- Generally, so far, we always have charged particles considered to be minimum ionising objects and photons as particles with a constant absorption coefficient. This is a rather good approximation for high energy particles. But as mentioned, for low energy particles the situation is more difficult, and tendentially, the energy loss by ionisation and the photon absorption coefficient rise. Moreover, electrons and positrons, which have been treated equally here, do not always show exactly the same behaviour inside matter.

Therefore, the configuration of a real Si strip detector should be implemented into GEANT4 and it should be analysed which signals the particles really induce inside the detector.

6 Conclusions

In this project, Compton Backscattering for measuring the ILC beam energy has been studied using GEANT4. The simulations were performed for $E_b = 250GeV$, $\omega_L = 1.165eV$ (Nd:YAG), the magnet parameters l=3m, B=0.28T and the magnet-detector distance L=50m. The distribution $\frac{dN}{dx}$ for the scattered electrons at the detector showed the Compton edge at x=28.3cm. However, the entries at the edge are low so that improvements for the statistics, like using the CO_2 laser or enlarging the luminosity, should be considered. More detailed studies should include beam energy and position smearing.

The Compton backscattered photons are intended to be used as a measure for the position of the original electron beam. Lorentzian or Gaussian ansatzes gave mean peak positions whose deviations from x=0, the expected value, were well below 1μm. It was discovered that SR produced by the electrons in the bending magnet (with an average multiplicity of about 5 photons per electron) constitutes a serious background. Due to their low energy in the MeV range, however, the peak position of the Compton photons (GeV range) could be extracted precisely enough from the $\frac{dE}{dx}$ distribution. Consequently, a photon calorimeter would be in principle a good detector option. However, further R&D in this field is necessary.

As an alternative, we propose to place a Pb absorber in front of the detector so that the Compton photons can convert into e+/e- particles which can be measured by a high resolution Si strip detector. The position of the e+/e- peak was found to reproduce the primary Compton photons peak very well. Moreover, for a 20mm thick absorber the e+/e- background produced by the SR was highly reduced. This enabled us to extract the peak position with a precision about $1\mu m$ if the background is well-known independently. It is expected that the background can be further minimised for larger absorber thicknesses or, alternatively, by a sweeping magnet placed between absorber and detector.

In order to check the validity of simplifying assumptions and to see which signals would be really generated inside the detector, a Si strip configuration should be implemented in future GEANT4 simulations.

With ongoing research, it should be achievable to measure the position of both the electron edge and the Compton photon peak or its e+/e- representation with a precision of 1μm or better. This would make the Compton backscattering method accurate enough to monitor the ILC beam energy with a precision of 10^{-4}.

Acknowledgements

This project was done during the DESY Zeuthen Summer School Programme 2006 under the supervision of Jürgen Schreiber. I would like to thank DESY and its staff for offering this programme and the very good organisation, Jürgen Schreiber and Michele Viti for the enjoyable and friendly cooperation and Martin Ohlerich for helpful tips. Furthermore, thanks a lot to the summerstudents and my girlfriend Gosia, who made this stay a great experience also after work.

References

[1] V.N. Duginov et al., The Beam Energy Spectrometer at the International Linear Collider, LC-DET-2004-031.

[2] K. Hiller, R. Makarov, H.J. Schreiber, E. Syresin and B. Zalikhanov, ILC Beam Energy Measurement based on Synchrotron Radiation from a Magnetic Spectrometer, Draft July 2006.

[3] R. Klein et al., Measurement of the BESSY II electron beam energy by Compton-backscattering of laser photons, Nucl. Inst. Meth. A486 (2001) 545.

[4] N. Muchnoi, VEPP-4M collider beam energy measurement by inverse Compton scattering of laser radiation, contribution to the ILC Energy Spectrometer Meeting, Dubna, May 2006.

[5] H. Paukkunen, Could Compton scattering be used for measuring the beam energy at the International Linear Collider?, Desy Zeuthen, September 2005.

[6] H.J. Schreiber, Precise ILC Beam Energy Measurement using Compton backscattering, contribution to the ILC Energy Spectrometer Meeting, Dubna, May 2006.

[7] K. Wille, The Physics of Particle Accelerators - An Introduction, Oxford University Press, 2000.

Appendix

A Fitting the Edge: Convolution of Two Linear Functions with a Gaussian

Let us consider the case of folding a step function, or more generally, two linear functions with a Gaussian as illustrated in Fig. 13. This ansatz can be considered a good description for the Compton edge behaviour of scattered electrons within a detector to monitor the pimary beam energy with high precision at an ILC.

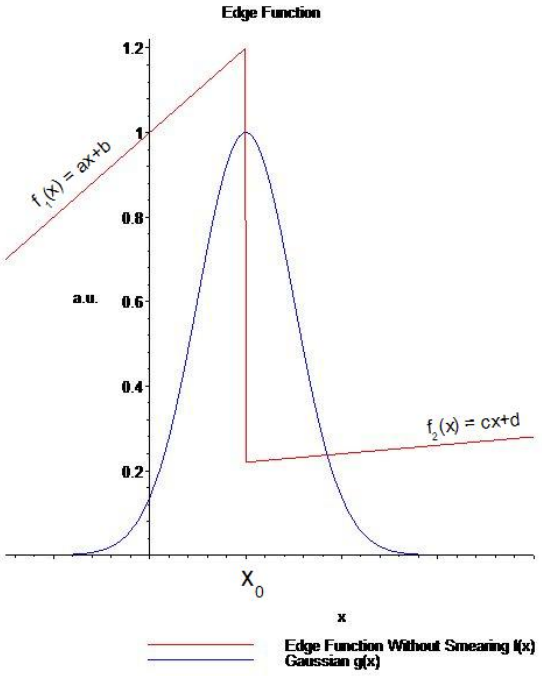

Figure 13: The linear functions and the Gaussian before folding.

The generalised step function can be written as:

$$f(x) = \begin{cases} f_1(x) \text{ for } x<x_0 \\ f_2(x) \text{ for } x>x_0 \end{cases} = \begin{cases} ax+b \text{ for } x<x_0 \\ cx+d \text{ for } x>x_0 \end{cases}$$

Gaussian:

$$g(x) = \frac{1}{\sigma\sqrt{2\pi}} e^{-\frac{(x-x_0)^2}{2\sigma^2}}$$

To simplify the calculations, we set $x_0 = 0$ in the following; to take into account non-zero values of x_0, the final result will be shifted manually by x_0.

For later use, we denote here the definitions and basic properties of the errorfunction erf and its complement erfc:

$$\begin{aligned}
\mathrm{erf}(t) &= \frac{2}{\sqrt{\pi}}\int_0^t e^{-x^2}dx \\
\mathrm{erfc}(t) &= 1-\mathrm{erf}(t) = \frac{2}{\sqrt{\pi}}\int_t^\infty e^{-x^2}dx = \frac{2}{\sqrt{\pi}}\int_{-\infty}^{-t} e^{-x^2}dx \\
\mathrm{erfc}(-t) &= \frac{2}{\sqrt{\pi}}\int_{-t}^\infty e^{-x^2}dx = 2\mathrm{erf}(t)+\mathrm{erfc}(t) = 2-\mathrm{erfc}(t)
\end{aligned}$$

Now we start to calculate the convolution of f(x) with g(x):

$$\begin{aligned}
f(t) &= \int f(x)g(x-t)dx \\
&= \int_{-\infty}^0 f_1(x)g(x-t)dx + \int_0^\infty f_2(x)g(x-t)dx \\
&= \frac{a}{\sigma\sqrt{2\pi}}\underbrace{\int_{-\infty}^0 xe^{-\frac{(x-t)^2}{2\sigma^2}}dx}_{I_1} + \frac{b}{\sigma\sqrt{2\pi}}\underbrace{\int_{-\infty}^0 e^{-\frac{(x-t)^2}{2\sigma^2}}dx}_{I_2} + \frac{c}{\sigma\sqrt{2\pi}}\underbrace{\int_0^\infty xe^{-\frac{(x-t)^2}{2\sigma^2}}dx}_{I_3} + \frac{d}{\sigma\sqrt{2\pi}}\underbrace{\int_0^\infty e^{-\frac{(x-t)^2}{2\sigma^2}}dx}_{I_4}
\end{aligned}$$

- I_1: With the aid of the substitution $u=(\frac{x-t}{\sqrt{2}\sigma})^2 \Rightarrow \frac{du}{dx}=\frac{x-t}{\sigma^2} \Rightarrow xdx=\sigma^2du+tdx$, and later $v=\frac{x-t}{\sqrt{2}\sigma} \Rightarrow dv=\frac{dx}{\sqrt{2}\sigma}$, one obtains for I_1:

$$\begin{aligned}
I_1 &= \int_{-\infty}^0 xe^{-\frac{(x-t)^2}{2\sigma^2}}dx = \int_{-\infty}^{\frac{t^2}{2\sigma^2}} e^{-u}\sigma^2du + \int_{-\infty}^0 te^{-\frac{(x-t)^2}{2\sigma^2}}dx = \left[-e^{-u}\sigma^2\right]_{\infty}^{\frac{t^2}{2\sigma^2}} + \int_{-\infty}^{-\frac{t}{\sqrt{2}\sigma}} e^{-v^2}\sqrt{2}\sigma t dv \\
&= -\sigma^2e^{-\frac{t^2}{2\sigma^2}} + \sigma t\frac{\pi}{\sqrt{2}}\ \mathrm{erfc}(\frac{t}{\sqrt{2}\sigma})
\end{aligned}$$

- I_2: By means of the substitution $v=\frac{x-t}{\sqrt{2}\sigma}$, one obtains for I_2:

$$I_2 = \int_{-\infty}^0 e^{-\frac{(x-t)^2}{2\sigma^2}}dx = \sqrt{\frac{\pi}{2}}\sigma\ \mathrm{erfc}(\frac{t}{\sqrt{2}\sigma})$$

- I_3: The calculation of I_3 is analogous to the one of I_1, only the endpoints of the integral are different:

$$I_3 = \int_0^\infty xe^{-\frac{(x-t)^2}{2\sigma^2}}dx = \sigma^2e^{-\frac{t^2}{2\sigma^2}} + \sqrt{\frac{\pi}{2}}\sigma t\ \mathrm{erfc}(-\frac{t}{\sqrt{2}\sigma}) = \sigma^2e^{-\frac{t^2}{2\sigma^2}} + \sqrt{2\pi}\sigma t - \sqrt{\frac{\pi}{2}}\sigma t\ \mathrm{erfc}(\frac{t}{\sqrt{2}\sigma})$$

- I_4: Finally, I_4 is calculated similarly to I_2:

$$I_4 = \int_0^\infty e^{-\frac{(x-t)^2}{2\sigma^2}}dx = \sqrt{\frac{\pi}{2}}\sigma\ \mathrm{erfc}(-\frac{t}{\sqrt{2}\sigma}) = \sqrt{2\pi}\sigma - \sqrt{\frac{\pi}{2}}\sigma\ \mathrm{erfc}(\frac{t}{\sqrt{2}\sigma})$$

With these results for the integrals, the convolution $f(t)$ can be written

$$\begin{aligned} f(t) &= -\frac{a\sigma}{\sqrt{2\pi}}e^{-\frac{t^2}{2\sigma^2}} + \frac{at}{2}\ \mathrm{erfc}(\frac{t}{\sqrt{2}\sigma}) \\ &\quad +\frac{b}{2}\ \mathrm{erfc}(\frac{t}{\sqrt{2}\sigma}) \\ &\quad +\frac{c\sigma}{\sqrt{2\pi}}e^{-\frac{t^2}{2\sigma^2}} + ct - \frac{ct}{2}\ \mathrm{erfc}(\frac{t}{\sqrt{2}\sigma}) \\ &\quad +d - \frac{d}{2}\ \mathrm{erfc}(\frac{t}{\sqrt{2}\sigma}) \\ &= \frac{\sigma}{\sqrt{2\pi}}(c-a)e^{-\frac{t^2}{2\sigma^2}} + \frac{1}{2}((a-c)t + (b-d))\ \mathrm{erfc}(\frac{t}{\sqrt{2}\sigma}) + ct + d \end{aligned}$$

If needed, a shift by x_0 along the x-axis has to be performed: $t \rightarrow t - x_0$ so that the final result is

$$f^*(t) = \frac{\sigma}{\sqrt{2\pi}}(c-a)e^{-\frac{(t-x_0)^2}{2\sigma^2}} + \frac{1}{2}((a-c)(t-x_0) + (b-d))\mathrm{erfc}(\frac{t-x_0}{\sqrt{2}\sigma}) + c(t-x_0) + d$$